Understanding Electrochemical Reversibility using Density Functional Theory: Bridging Theoretical Scheme of Squares and Experimental Cyclic Voltammetry

Amir Mahdian[1], Arsalan Hashemi[1],* and Kari Laasonen[1]†
[1] *Department of chemistry and material science, School of chemical engineering, Aalto University, 02150 Espoo, Finland*

Mechanistic redox and acid-base reactions play pivotal roles in numerous applications in both chemistry and biology. Bridging the gap between computational insights and experimental observations is crucial to illuminate the mechanisms underlying these redox processes. In this study, we enhanced our understanding of electrochemical reactions by leveraging the scheme of squares framework using a set of tens of molecules that have been examined in the field of redox flow batteries. Furthermore, we focused on developing our computational models by calibrating the calculated redox potentials against experimental data, thereby enhancing the predictive performance of our approach. These findings are applicable to a wide range of applications from energy storage to medicine and synthetic chemistry.

I. INTRODUCTION

The study of electron transfer and its role in chemical reactions is fundamental to the functionality of various electrochemical devices including batteries, fuel cells, and electrolysis systems [1–6]. To enhance the performance of these applications, a thorough understanding of the energy pathways within the reaction mechanism is required. Accordingly, both kinetics and thermodynamics analyses are essential for optimizing electrochemical reactions, and the kinetics of these processes are often governed by underlying thermodynamic principles [7, 8].

In flow batteries [9, 10], *reversible* electrochemical reactions are essential for facilitating successful charging and discharging. Full reversibility is achieved when electrons are transferred back and forth at nearly identical kinetic rates under similar electrode potentials. However, redox reactions are not the only reactions that occur [11]; various side reactions, such as acid-base reactions [12] and disproportionation [13] can also occur, adding complexity to the mechanism and potentially introducing irreversibility into the desired redox reaction.

An acid-base reaction is a chemical process in which an acid donates a proton (H^+) to a base, forming a conjugate base and a conjugate acid. When this reaction occurs alongside a redox reaction, it can alter the mechanistic nature of the overall process and impact the quantitative results [14]. Consequently, understanding this combinatory reaction at a microscopic level is crucial. This is achieved by assessing the equilibrium states when a molecule is introduced into a solvent and/or an external potential is applied. The key is to identify the reaction pathway that alters the chemistry, whether it is a decoupled electron transfer (ET) and proton transfer (PT) or a coupled (simultaneous) proton-electron transfer (PET) [15, 16].

Cyclic voltammetry (CV) is one of the most widely used techniques for characterizing redox-active systems [17–20]. This involves applying a potential to an electrode relative to a fixed reference potential, such as the standard hydrogen electrode (SHE) [21]. The potential varies linearly over time within the electrochemical potential window of the electrolyte. As an indicator of the number of electrons transferred, the current is measured simultaneously. Therefore, it is possible to determine the number of oxidation states and their stability, reaction rates, redox potentials, and concentrations of redox-active species [22].

As with other experimental methods, it can be challenging to obtain atomic-level details, particularly when studying solid-liquid interfaces. Consequently, computational analyses are essential for gaining a deeper understanding of electrochemical properties and redox mechanisms, which are typically difficult to observe directly. This aids in refining the experimental design and interpreting the results.

Through electrochemical reaction analyses, the kinetics assessments, however, require additional computational resources or model simplification [23–25]. The thermodynamic data are easily evaluated by determining the changes in the Gibbs free energy (ΔG) of the reactants and products. In the prediction of a combined redox and acid-base reaction, three potential mechanisms, ET, PT, and PET, are systematically diagrammed along the sides and diagonal of a square, forming a representation known as an *electrochemical scheme of square* [26–28]. This diagram effectively elucidates the mechanistic pathways and redox potentials for multi-electron and multi-proton transfer reactions as functions of the applied electrode potential and the electrolyte pH.

Density functional theory (DFT) approach [29, 30] in combination with implicit solvation models [31] and a computational standard hydrogen electrode (SHE) [32] are frequently used to simulate electrochemical environments. Despite their widespread use, these methods face challenges, including the accurate modeling of charged systems, capturing the dynamic and electrostatic effects of electrodes, and addressing deficiencies in basis sets and exchange-correlation (XC) functionals [33]. These limitations often lead to significant discrepancies, for example,

* arsalan.hashemi@aalto.fi
† kari.laasonen@aalto.fi

in the Gibbs free energy, compared to the experimental values [34].

To address this issue, one might calibrate the DFT outputs to align them with the corresponding experimental results. This adjustment should eliminate discrepancies and indirectly incorporate the experimental effects into the calculated values. Generally, the validity and diversity of the collected data are crucial. For instance, our group [35], along with others [36–38], scaled theoretical pK_a values to match experimental values in various solvents for organic molecules. Hamza et al. [39] recently adjusted the electron transfer (ET) redox potentials to predict the properties of pyridinium derivatives. Yet, benchmarks of redox potentials are still lacking for species of various families that undergo redox reactions via different mechanisms.

In what follows, we explain how the electrochemical scheme of squares can be employed to interpret and predict the experiments. We also addressed the absence of scaled redox potentials for the ET and PET reactions. To this end, a systematic effort was made to establish a relationship that reconciles the discrepancies between the theoretical predictions and experimental measurements. This approach not only deepens our understanding of redox behavior but also establishes a foundational framework for accurately predicting the electrochemical properties of new molecular systems in other related fields of research.

II. CRITERIA FOR ELECTROCHEMICAL REVERSIBILITY

A. Redox Potential

As mentioned earlier, the CV technique measures the relationship between the potential and current resulting from electrochemical reactions occurring at the working electrode surface. These reactions can be exemplified by the following *reduction* process:

$$[\text{electrode}]^{n} + \text{X}^{m} \rightarrow [\text{electrode}]^{n-n_e} + \text{X}^{m+n_e} \quad (1)$$

In this reaction, n and m represent the numbers of electrons in the electrode and molecule X, respectively. Additionally, n_e represents the number of electrons transferred from the electrode to X during the redox reaction. A reverse reaction, known as *oxidation*, can also be considered.

During the redox (*reduction-oxidation*) process, each species may also undergo proton (H^+) transfer reactions:

$$\text{X}^{m} + n_p\text{H}^{+} \rightarrow [\text{XH}_{n_p}]^{m-n_p}. \quad (2)$$

Here, n_p represents the number of protons involved in the acid-base reactions. This reaction may occur sequentially or simultaneously with the ET reaction. The sequence of reactions can vary, and several meta-stable states can be formed depending on the number of electrons and protons involved. Figure 1 illustrates various mechanisms for one-electron, one-proton transfer reactions.

When the electrode potential is applied, the current peaks as a function of the ratio of the activities of the oxidized (ox) and reduced (red) species at the potential E:

$$E = E^0_{\text{ox/red}} + \frac{RT}{n_eF}\ \ln\left(\frac{a_{\text{ox}}}{a_{\text{red}}}\right) \quad (3)$$

This equation is referred to as the Nernst equation [40]. Here, $E^0_{\text{ox/red}}$ is based on the standard potential, which is equal for both reduction and oxidation reactions. The parameter a_i, which denotes the activity of species i, is defined as:

$$a_i = \gamma_i(c_i/c^0_i),$$

where γ_i is a dimensionless activity coefficient, c_i is the concentration of species i, and c^0 represents the standard concentration. The symbols T, F, and R represent the temperature (in K), the Faraday constant, and the universal ideal gas constant, respectively.

Now, let us consider how different reactions impact E:
PT reaction: Proton is driven by the solution, it thus depends solely on the acidity constant of the active species and pH of solution. This reaction is a chemical reaction and proceeds without any direct electrode involvement.
ET reaction: Assuming a 1:1 ratio for the ET reactions (all oxidized species are fully reduced and/or vice versa) allows us to disregard the second term of Equation (3), simplifying it to $E = E^0_{\text{ox/red}}$ (because $\ln 1 = 0$). Furthermore, $E^0_{\text{ox/red}}$ represents the redox potential for the transfer of n_e electrons and is defined by the following equation:

$$E^0_{\text{ox/red}} = -\frac{\Delta G_{\text{ox/red}}}{n_eF} = -\frac{\Delta G_{\text{X}^m/\text{X}^{m+n_e}}}{n_eF} \quad (4)$$

Here, $\Delta G_{\text{X}^m/\text{X}^{m+n_e}}$ denotes the change in the Gibbs free energy associated with the ET reactions.
PET reaction: When H^+ ions are also involved in the redox reactions, it becomes crucial to define the formal potential for the overall reaction rather than just for the ET reaction:

$$[\text{electrode}]^{n} + \text{X}^{m} + n_p\text{H}^{+} \rightarrow [\text{electrode}]^{n-n_p} + [\text{XH}_{n_p}]^{m+n_e-n_p}. \quad (5)$$

In such a reaction, the activity of H^+ is conventionally set to 1 to determine $E^0_{\text{ox/red}}$. Equation (4) is used again, but in this instance, with $\Delta G_{\text{X}^m/[\text{XH}_{n_p}]^{m+n_e-n_p}}$. In simple terms, the redox potential is initially determined for a pH of 0.

The activity of the H^+ species can be adjusted by the pH of the solution, as described by the following equation:

$$\text{pH} = -\log(a_{\text{H}^+}) \quad (6)$$

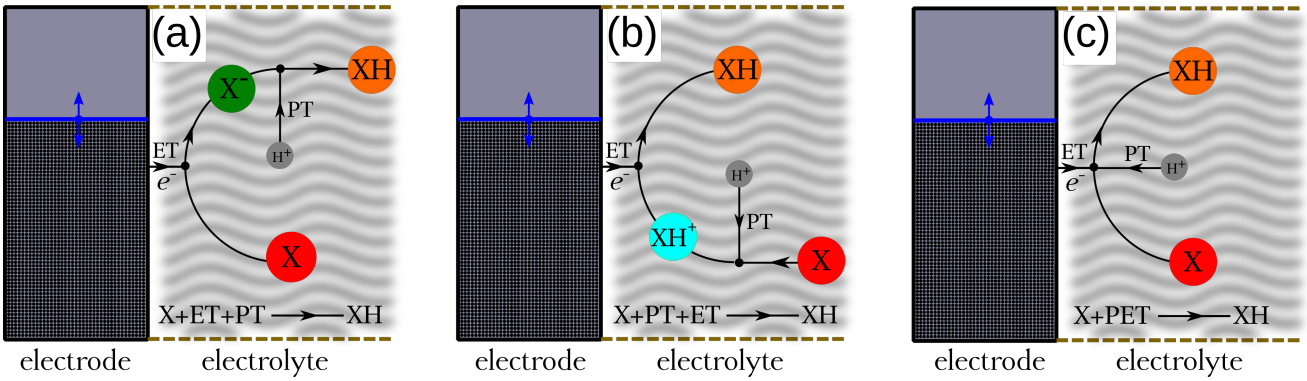

Figure 1. Schematic representation of the reduction reaction of molecule X adjacent to an electrode through various mechanisms: X is converted into XH via (a) sequential electron transfer (ET) followed by proton transfer (PT); (b) sequential proton transfer (PT) followed by electron transfer (ET); and (c) simultaneous proton-electron transfer (PET) reactions. Electrode energy level (blue line) can be adjusted to source electron for the favored reaction.

Consequently, the activity a_{H^+} is determined as:

$$a_{\mathrm{H}^+} = 10^{-\mathrm{pH}} \tag{7}$$

In scenarios where there are n_p protons involved (as outlined in Eq. 5), the activity ratio can be expressed as:

$$\frac{a_{\mathrm{ox}}}{a_{\mathrm{red}}} = \frac{a_{\mathrm{X}^m} \cdot [a_{\mathrm{H}^+}]^{n_p}}{a_{[\mathrm{XH}_{n_p}]^{m+n_e-n_p}}}, \tag{8}$$

Integrating Equations (3), (7), and (8), the Nernst equation can be reformulated for our specific system as follows:

$$E = E^0_{\mathrm{X}^m/[\mathrm{XH}_{n_p}]^{m+n_e-n_p}} - \left(\frac{n_p RT\ln(10)}{n_{el}F}\right)\mathrm{pH}. \tag{9}$$

At approximately room temperature, the value of $RT\ln(10)/F$ is approximately 0.059 eV.

B. Current-Potential Relationship

The rates of the reduction and oxidation reactions are expressed as follows:

$$\nu_{\mathrm{red}} = k_{\mathrm{red}}\ c_{\mathrm{ox}}(0,t) = j_c/n_eF \tag{10}$$

$$\nu_{\mathrm{ox}} = k_{\mathrm{ox}}\ c_{\mathrm{red}}(0,t) = j_a/n_eF, \tag{11}$$

where ν_{red} and ν_{ox} represent the rates of reduction and oxidation reactions, j_c and j_a represent the partial cathodic and anodic current densities, respectively. The cathodic current involves electron transfer from an electrode to a species in solution, whereas the anodic current involves electron transfer from a species in solution to an electrode. The terms $c_{\mathrm{ox}}(0,t)$ and $c_{\mathrm{red}}(0,t)$ denote the concentrations of oxidized and reduced forms at the electrode surface, respectively, at time t. Under steady-state conditions, these concentrations are not time-dependent. Additionally, k_{ox} and k_{red} denote the oxidation and reduction rate constants, respectively.

However, if the system is not in equilibrium, the current will flow as described by the following equation:

$$\nu = k_{\mathrm{red}}\ c_{\mathrm{ox}}(x=0) - k_{\mathrm{ox}}\ c_{\mathrm{red}}(x=0) = j/n_eF. \tag{12}$$

For any chemical reaction, the rate constant is related to the Gibbs free energy of activation ($\Delta G^\dagger$) using the Arrhenius equation as follows:

$$k = k_{max}\ \exp(-\Delta G^\dagger/RT), \tag{13}$$

where k_{max} denotes the upper limit of k.

For a symmetric current-potential diagram, the potential dependence of the rate constants can be expressed as follows:

$$k_{\mathrm{red}} = k_{\mathrm{max}}\ \exp\Big[-n_eF(E_{\mathrm{appl}} - E^0_{\mathrm{ox/red}})/2RT\Big] \tag{14}$$

$$k_{\mathrm{ox}} = k_{\mathrm{max}}\ \exp\Big[n_eF(E_{\mathrm{appl}} - E^0_{\mathrm{ox/red}})/2RT\Big]. \tag{15}$$

Here, E_{appl} represents the electrode's applied potential.

At equilibrium, the electrochemical current j is equal to zero, $j_a = |j_c| = j_0$ (indicating dynamic equilibrium) and no difference exists between the surface and bulk concentrations. By integrating Eqs. (14 and 15) into Eq. (12), one derives

$$n_eF\ (E_{\mathrm{appl}} - E^0_{\mathrm{ox/red}})/RT = c_{\mathrm{ox}}/c_{\mathrm{red}} \tag{16}$$

Finally, the expression for j_0 as a function of E_{appl} is given by

$$j_0 = -n_eFk_{max}\ c_{\mathrm{ox}}\ \exp[-\alpha n_eF(E_{\mathrm{appl}} - E^0_{\mathrm{ox/red}})/RT], \tag{17}$$

where α is the transfer coefficient. For a symmetric barrier, $\alpha = 0.5$, but generally ranges from 0 to 1.

C. Reversible Electrochemical Reactions using Scheme of Squares

Electrochemical reversibility implies that a redox reaction occurs rapidly in both anodic and cathodic current directions at almost the same rate. In this case, the activation energy is low. According to Eq. (17), this is possible when $E_{\text{appl}} = E^0_{\text{ox/red}}$. The applied potential E_{appl} can be controlled within the solvent potential window (E_w). This facilitates the regulation of the reaction rate within these limits, while avoiding any further unintentional side reactions. For aqueous solutions, E_w value is between -1.5 V and $+1.5$ V [41].

To achieve reversibility, it is necessary for the concentrations of both reduced and oxidized species to be similar. This ensures that the deviation between the cathodic current potential peak (E^0_{red}) in Eq. 14 and the anodic current potential peak (E^0_{ox}) as described in Eq. 15 is minimized. We propose that the oxidation reaction proceeds via the reverse of the reduction reaction through the same pathway to achieve this alignment. It avoids a strong deviation of the activity coefficient ratio from unity (cf., Eq. 8).

Indeed, there should be no adsorption or other types of side reactions, high structural reorganization energy, and so on. This information is beyond the scope of the scheme of square representation. Some of the irreversible molecules and molecule that has discrepancies between experimental and theoretical can be found in Supplementary Information (SI).A completely irreversible reaction only shows one peak, that is, the reduction peak when the oxidized form is present in the solution. In this case, the anodic and cathodic reactions are never simultaneously significant.

III. COMPUTATIONAL FRAMEWORK

All DFT calculations were conducted using the Gaussian 16 software [42]. Molecular geometry optimization was conducted using two separate sets of calculations: (i) the 6-31G(d) basis set [43] combined with the M06-2X functional [43] and (ii); the PM7 semiempirical method [44], both of which incorporate SMD solvation [45]. The frequency data were subsequently calculated at the same level of analysis. For total energy, the Def2TZVP basis set [46], coupled with the M06-2X functional, was utilized to perform single-point energy calculations. Finally, the Gibbs free energy was determined by adding relevant quantities. We will refer to these two sets of calculations as 6-31G(d)-Def2TZVP and PM7-Def2TZVP.

Generally, the reactions can be represented by the following equation (assuming $n_p \approx n_e$):

$$\mathrm{XH}_n \rightleftharpoons [\mathrm{XH}_{n-n_p}]^{n_e} + n_p\mathrm{H}^+ + n_e\mathrm{e}^-, \tag{18}$$

As previously discussed, the necessary protons (H^+) are sourced from an aqueous solution, while the electrons (e^-) are derived from an electrode.

To assess the thermodynamics of the reaction, it is essential to determine the Gibbs free energy of each state involved in the process. The Gibbs free energies of the XH_n and $[\mathrm{XH}_{n-n_p}]^{n_e}$ species can be readily analyzed, while the energetics of H^+ and e^- prove to be more complex. To address this issue, two following reactions are essential:
(i) The standard potential of the hydrogen electrode, as the reference electrode, is 0 V for the reaction written as

$$\frac{1}{2}\mathrm{H}_2(\mathrm{g}) \rightleftharpoons \mathrm{H}^+(\mathrm{aq}) + \mathrm{e}^-. \tag{19}$$

(ii) An experimental pK_a as a reference to capture $H^+(aq)$ Gibbs free energy. Herein, formic acid (HCOOH) dissociation reaction with $pK_a^{ref.} = 3.77$ is employed [47]:

$$\mathrm{HCOOH} \Longrightarrow \mathrm{HCOO}^- + \mathrm{H}^+. \tag{20}$$

The logarithm of acidity constant (K_a), represented by the pK_a value, is defined as:

$$\mathrm{p}K_a = \frac{\Delta G_{\mathrm{PT}}}{RT\ln(10)}. \tag{21}$$

Therefore, the reference Gibbs free energy change for the reaction (20), denoted as $\Delta G^{ref.}_{\mathrm{PT}}$, is calculated to be 0.224 eV.

The calculation of the Gibbs free energies for HCOOH and $HCOO^-$ can be easily performed. We determined that the Gibbs free energy of the solvated proton, denoted by $G_{\mathrm{H^+(aq)}}$, is -11.798 eV. Referring back to Equation (19), we can compute that $G_{\mathrm{e^-}} = -4.115$ eV.

Subsequently, the obtained pK_a values need to be adjusted to address limitations inherent in the implicit solvation model used in our study[35], as described below:

$$\mathrm{p}K_a{}^{scaled} = 0.49\ \mathrm{p}K_a + 3.2 \tag{22}$$

As previously noted, no scaling formula has been established for the redox potentials of the ET and PET reactions that fit our computational setup. In the present study, we delineated these relationships.

IV. RESULTS AND DISCUSSION

A. Scheme of Squares Usage

1. *Fluorenone derivatives*

Carboxylic acid (CA)-functionalized 9-fluorenone (FL), (see Figure 2 (a)), was tested under alkaline conditions (1M KOH, pH = 14) with various positional configurations of CA [48]. The modified FLs were named based on their structural modifications: 9-fluorenone-1-carboxylic acid (FL-1CA), 9-fluorenone-2-carboxylic acid (FL-2CA), 9-fluorenone-3-carboxylic acid (FL-3CA), and 9-fluorenone-4-carboxylic acid (FL-4CA).

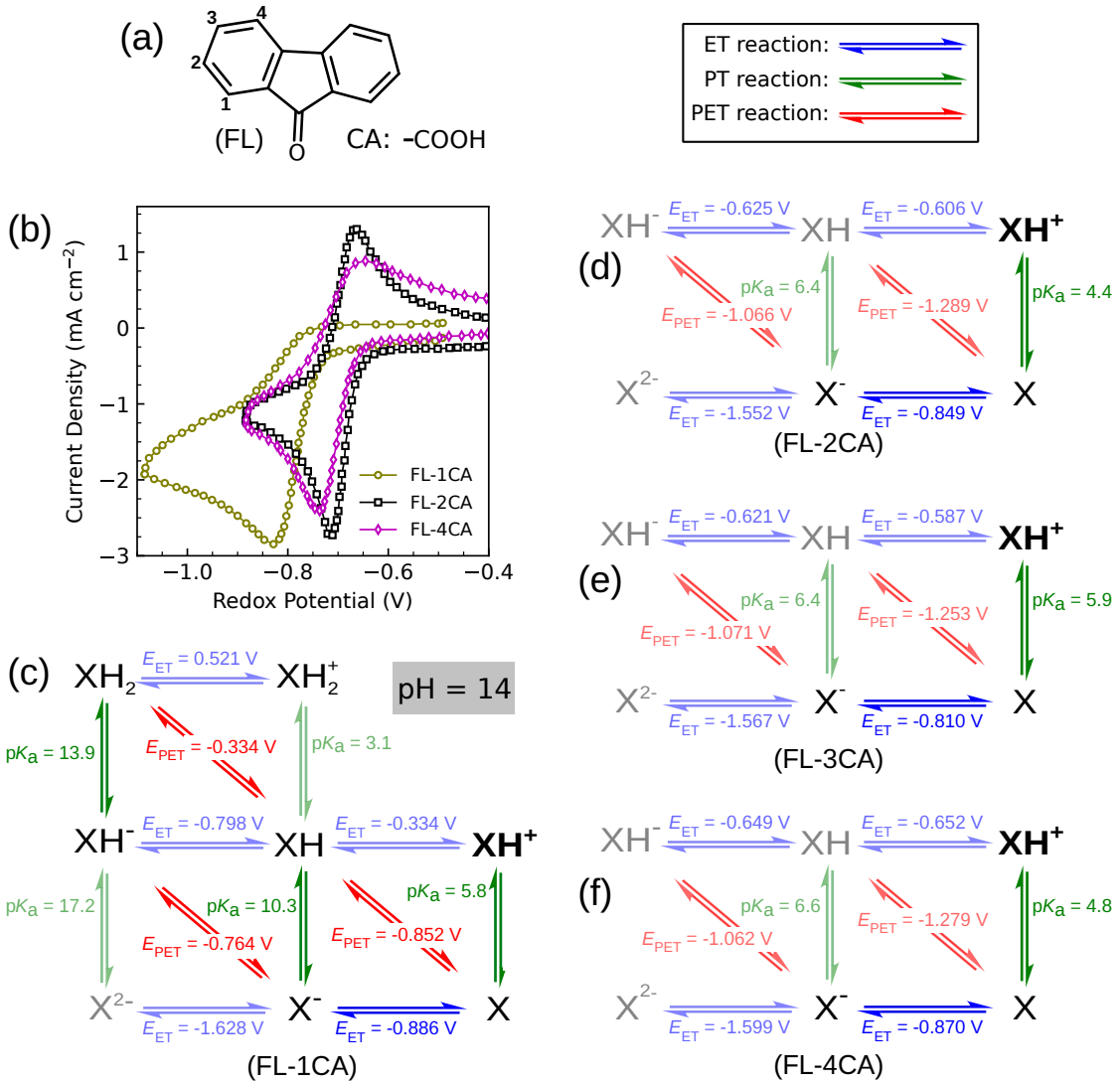

Figure 2. (a) Graphical representation of 9-fluorenone (FL) with numbered functionalization sites. (b) Experimental cyclic voltammetry (CV) measurements were conducted on 10 mM solutions of carboxylic acid-functionalized FL compounds in 1M KOH. The scan rate was set at 100 mV/s, as reported in Rodriguez et al. [48]. The compounds are named FL-1CA, FL-2CA, and FL-4CA. (c-f) Electrochemical scheme of squares of 9-fluorenone derivatives (FL-nCA) including FL-1CA, FL-2CA, FL-3CA, and FL-4CA, at a pH of 14. Vertical, horizontal, and diagonal arrows indicate PT, ET, and PET reactions, respectively. PT is gauged by pK_a, while ET and PET are assessed by redox potentials in V_{SHE}, with PET potentials adjusted for a pH of 14. $\mathbf{XH}^+$ represents the initial compound before equilibration (deprotonation).

Electrochemical tests of the FL-1CA, FL-2CA, and FL-4CA isomers are shown in Figure 2(b). The FL-1CA compound underwent an irreversible reaction, whereas FL-2CA and FL-4CA both showed reversiblity. FL-1CA was reduced at a lower reduction potential (≈ -0.812 V), indicating it was difficult to reduce compared to FL-2CA and FL-4CA, which both had almost similar reduction potentials of approximately -0.69 V. The data also indicated that a wider range of electrode potential was used in the CV analysis of FL-1CA.

Adding the CA functional group increases the solubility of the compounds but also makes them more likely to undergo PT reactions during the stabilization process before starting CV measurements. FL-nCA derivatives can release H^+ depending on the pH of the environment. If the compound is more acidic than its surroundings, it acts as a donor, releasing hydrogen ions and transforming -COOH into a -COO$^-$.

The calculated pK_a values for FL-1CA, FL-2CA, FL-3CA, and FL-4CA are 5.8, 4.4, 5.9, and 4.8, respectively, as shown in Figures 2 (c-f). The initial compound in each scheme is denoted as $\mathbf{XH}^+$. These values indicate that these compounds are acidic and can easily lose a proton under alkaline conditions. $\mathbf{XH}^+$ is converted into X. The release of protons into the solution could lower the pH, especially if the concentration of active compounds

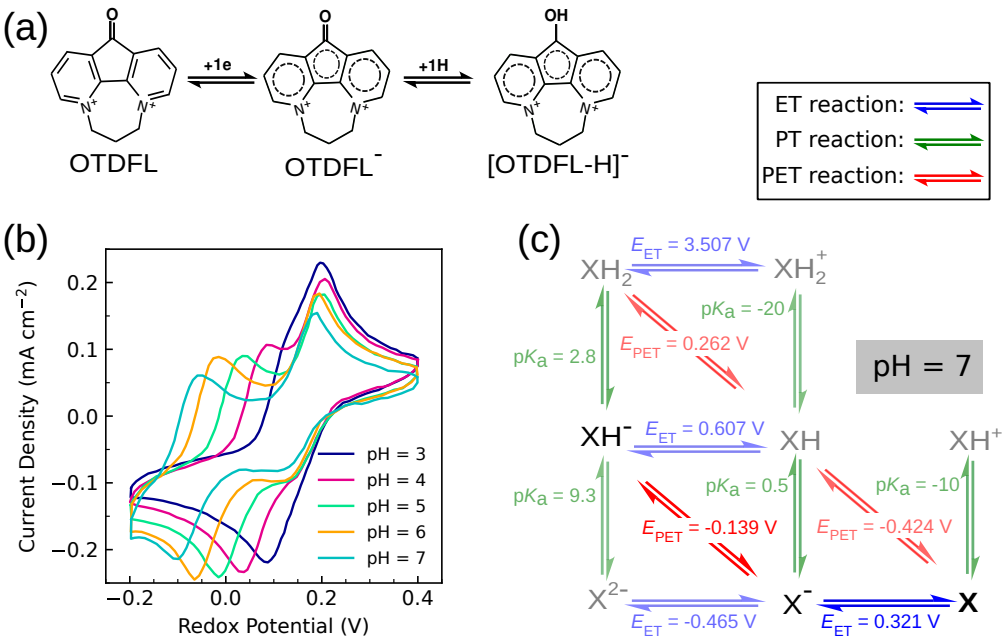

Figure 3. (a) OTDFL participates in the ET and PET reactions during the reduction process. The oxygen atom in the ketone group is protonated. (b) Experimental cyclic voltammetry of OTDFL at different pH values from 3 to 7, taken from Ref. [49]. (c) The electrochemical scheme of the squares of OTDFL at pH 7. Vertical, horizontal, and diagonal arrows indicate the PT, ET, and PET reactions, respectively. PT is gauged by pK_a, whereas ET and PET are assessed by redox potentials in V, with PET potentials adjusted for the corresponding pH. The redox potential was referenced to SHE. **X** represents the OTDFL.

is high.

It is important to note that when -COOH is positioned next to the ketone group (C=O), it can form an internal hydrogen bond, significantly altering the electrochemical properties of the compound. As illustrated in Figure S1, the FL-1CA-H radical (that is XH form) is more stable than the other isomers. This increased stability reduces its acidic nature. Specifically, it is less likely to lose a proton (to get deprotonated). Overall, a planar structure is more favorable for all species in their XH radical form.

To analyze the CV diagrams, one should begin with the deprotonated form of species X. The redox reaction of FL-1CA is irreversible, exhibiting only one peak at pH 14. This indicates that it can be reduced but cannot be oxidized back to its original state. Figure 2 (c) shows that X participates in two distinct reactions at similar redox potentials: ET and PET. For example, if X undergoes a PET reaction and forms an XH radical, it can evolve into either XH^-, XH_2, or X^-. The first two pathways involve reduction, while the third involves a deprotonation reaction. Conversely, if X forms X^- radicals via an ET reaction, the subsequent step is a PET reaction, in which XH^- equilibrates with XH_2. The predominant pathway is determined by the reaction kinetics. However, the presence of multiple reactive species in the solution not only reduces the oxidation rate but may also increase the likelihood of side reactions.

The placement of the -COOH group at sites 2, 3, and 4 completely changed the reaction mechanism. Only one reaction can occur: the formation of X^- from X. The X-to-XH pathway is blocked because at a pH of 14 it is hard to source H^+. Applying more potential could push the PET reaction to occur in the range of -1.062 to -1.071 V. In the experiment, the applied potential was increased to -0.9 V, therefore only one peak is expected.

This example shows that internal hydrogen bond formation can dramatically change mechanistic reaction pathways. Consequently, the characteristics of the redox-active species are affected. Indeed, the equilibration process is important before computing the redox pathways via the scheme of squares; the deprotonation reaction may proceed as soon as the species is introduced into the solution.

2. *Pyridinium-functionalized Fluorenone*

Li et al.[49] conducted detailed electrochemical surveys to elucidate the electrochemical mechanisms and structural transformations of OTDFL during its redox process. OTDFL, an acronym for *4-oxo-4,8,9,10-tetrahydro-7a,10a-diazacyclohepta[def]fluorene-7a,10a-diium*, undergoes a two-step electron transfer involving distinct reaction mechanisms: initially ET followed by PET (see Figure 3 (a)).

The CV experiments were conducted using 1 mM OTDFL at various pH values. The redox potential for the initial redox process remained untouched at 0.16 V. In contrast, the redox potential for the subsequent redox

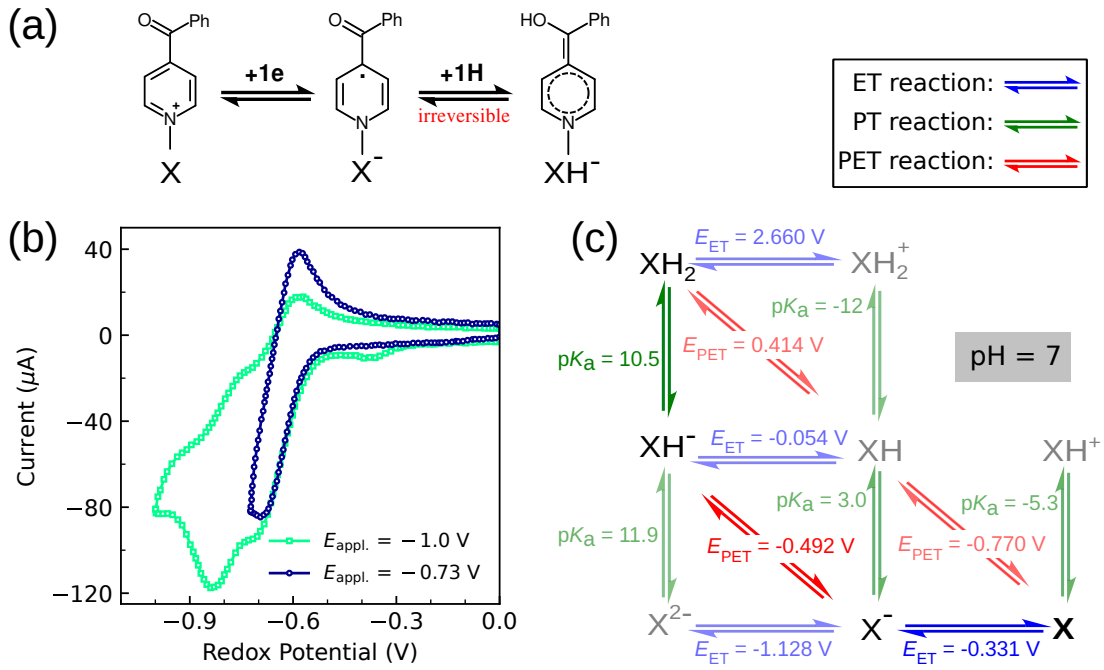

Figure 4. BenPy participates in the ET and PET reactions during the reduction process when a potential of up to -1 V is applied. (b) Experimental cyclic voltammetry of BenPy at different applied potentials -0.73 and -1 V versus SHE, taken from Ref. [50]. (c) The electrochemical scheme of the squares of BenPy at pH 7. Vertical, horizontal, and diagonal arrows indicate the PT, ET, and PET reactions, respectively. PT is gauged by pK_a, whereas ET and PET are assessed by redox potentials in V, with PET potentials adjusted for the corresponding pH. The redox potential was referenced to SHE. **X** represents the BenPy.

process exhibited a downward shift from 0.12 V to -0.09 V as the pH increased from 3 to 7. This pH-dependent variation in the second redox process demonstrated a slope of 0.059 V per pH unit, indicative of a PET reaction (Figure 3 (b)). Consequently, a single peak with a slight shoulder evolves into a two-peak diagram, where the higher-potential-positioned peak is always fixed. All the reactions were reversible.

Our scheme of squares (see Figure 3 (c)) elucidates the following aspects of the redox reactions: (i) no (de)protonation reaction occurs during the stabilization phase, leaving the system unchanged; (ii) the ET reaction predominates across all pH levels; (iii) the second electron transfer proceeds via a PET reaction, influencing the redox potential downshifts in response to the pH increases; (iv) the pathway X-to-X^--to-XH^- remains robustly consistent throughout the redox processes; (v) at pH values less than 2.8 or greater than 9.3, redox reactions should not be reversible, terminating at XH_2 in acidic conditions or X^{2-} under alkaline conditions; (vi) a discrepancy between experimental results and computational predictions, specifically a consistently larger gap in redox potentials, will be discussed in subsequent sections. The scheme of square for pH values of 3 and 6 can be found in the SI (Section III).

3. *Benzoylpyridinium*

In an experiment conducted by Sevov et al. [50], electron transfer occurred via the ET and PET reactions. The investigation concentrated on *1-Benzyl-4-methylpyridinium* (BenPy) within a 1M NaCl aqueous solution (refer to Figure 4 (a)).

The CV analysis exhibited two peaks at -0.63 and -0.73 V, yet with poor reversibility (Figure 4 (b), green trace). The conversion of X^- to XH^- involves the consumption of protons from the solution, increasing the pH from about 4 to 11. Nonetheless, adhering to a conservative CV sweep limit of -0.72 V prevented adverse second reduction, revealing a more reversible diagram (refer to Figure 4 (b), blue trace).

Furthermore, during the bulk electrolysis experiments, the dissolution of compound X^- in 1 M KOH (pH = 13.9) at room temperature without the application of any potential demonstrated no reactivity. Conversely, dissolving in a 0.1 M HCl (pH = 1.1) aqueous solution resulted in nearly instantaneous bleaching of the purple color of the radical. To provide further insight, X and XH undergo disproportionation reaction to form XH_2. However, the subject lies beyond the scope of this study.

Using the electrochemical scheme (see Figure 4 (c)), starting with species X at pH 7, a potential of -0.331 V is required to initiate the first ET reaction. Subsequently, the second electron is transferred at -0.492 V through a

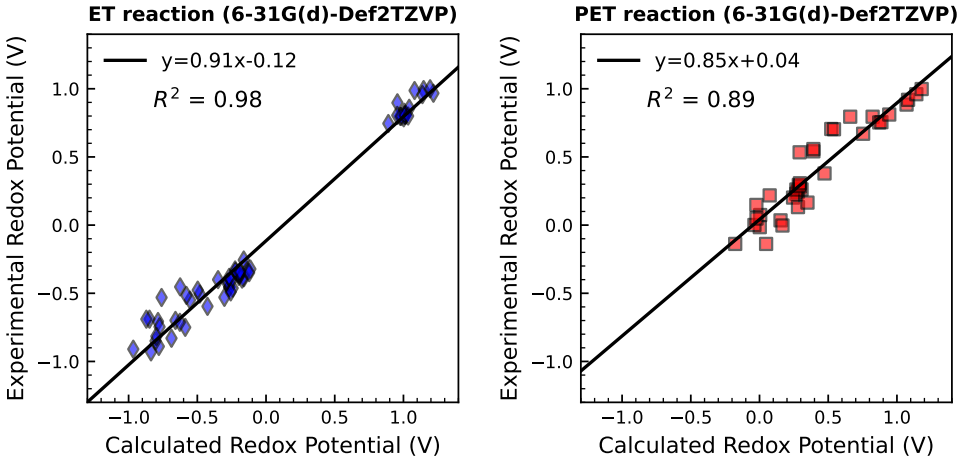

Figure 5. Scaling of calculated redox potentials of the ET and PET reactions against experimental data. Calculations were performed using 6-31G(d)-Def2TZVP computational setup. Each subplot includes the linear regression model formula along with the coefficient of determination (R^2).

PET mechanism, converting X^- to XH^-. Because this reaction is influenced by the pH, the redox potential becomes more negative as the pH increases. Eventually, compound XH^-, which displays stronger basic characteristics than the medium, can be protonated, forming species XH_2. The deprotonation reaction is no longer favored, and the system remains trapped in this state, unless the applied potential facilitates its reversibility through a PET reaction.

Given that the PET oxidation reaction (XH_2 to the XH path) is thermodynamically unfavorable, a much higher positive electrode potential is required. A comparison of the reduction and oxidation potentials highlights a significant overpotential, indicating that the reaction proceeds sluggishly and ultimately irreversibly.

Similar to the experiment, our calculations revealed a gap between the redox potentials of the ET (from X to X^-) and PET (from X^- to XH^-) reactions. However, similar to the previous example, the calculated potentials were overestimated, resulting in discrepancies with the experimental values. Thus, calibration of the calculated values against the experimental data becomes crucial.

B. Scaling Redox Potentials

The discrepancies between the calculated and experimental redox potential data were resolved by collecting redox potential data from the aqueous organic redox flow battery [51–53] literature, where CV analyses were performed. For each case, we examined the reaction pathway and collected the corresponding redox potential quantities (refer to SI for more details). The scheme of squares sheds light on which ET or PET reaction corresponds to the observed current peak (see Section V of the SI for more details). Note that the molecules considered for this purpose include quinones [54], phthalazines [55], phenazines [56], benzidines [57], TEMPO [58], and viologens [59].

For the PET reactions, the redox potentials were adjusted to a pH of 0 using the Nernst equation (Eq. (9)). All the experiments were performed at room temperature. In total, 60 and 36 samples were used to establish scaling relationships for ET and PET, respectively. A linear scaling relationship is used.

To calculate the scheme of squares, we considered two computational setups. First, a more precise M062X-Def2TZVP setup is suitable for single-case studies, owing to its higher resource demands. Second, an ultrafast PM7-M062X-Def2TZVP combination is used, which is crucial for large database generation, as we did previously [28]. Using this approach, geometry optimization and phonon calculations were conducted using the PM7 semi-empirical method. Subsequently, a single self-consistent field (SCF) iteration was performed to obtain the total energy term for Gibbs free energy calculations (see Section II of the SI for more details).

As shown in Figure 5, our computational setup demonstrated notable efficacy, particularly in the realm of ET reactions. Here, we report R^2 and scaling relations of 0.98 and $0.91E^0_{dft} - 0.12$, respectively. Our PET model has a small intercept value of 0.04 V. With a slope of 0.85, the calculations slightly overestimates the redox potential. The coefficient of determination is 0.89, indicating an acceptable level of reliability. In contrast to the alternative set of calculations (see Figure S2), where a different method was used for geometry optimization (DFT vs. semiempirical method), we observed only slight variations in the coefficients of the linear model. This outcome is consistent with findings reported in Ref. [35] regarding pK_a.

While utilizing scaling relationships will not change the reaction mechanisms, their inclusion will definitely make a better agreement between calculations and experiments.

V. CONCLUSION

Separating the composite PET reaction into distinct ET and PT reactions is experimentally unachievable and might be computationally infeasible depending on the methodology used. Additionally, virtual prescreening of organic molecules for various applications necessitates accurate redox potential assessments. This motivated us to investigate electrochemical square schemes and map them to experimental cyclic voltammograms. In conclusion, our study enhances the understanding of electrochemical pathways through thermodynamic profiles of PET reactions. This analysis allowed us to discern the pathways of the ET, PT, and PET reactions based on the reaction thermodynamics. The computationally simple yet rapid methodology employed effectively revealed reaction intricacies. With this insight, it is possible to address irreversibility issues by adjusting either the electrode potential or the solvent pH. Although kinetics may be significant in more complex cases, thermodynamic analysis provides valuable insights into the electrochemical reactions. To align the computational data with the experimental findings, we also calibrated the computed values using reliable experimental datasets. In summary, these findings can be applied to redox reactions and acid-base reactions across a wide range of scientific fields, including energy storage, medicine, and synthetic chemistry.

VI. ACKNOWLEDGMENT

This project has received funding from the European Union – NextGenerationEU instrument via Research Council Finland under grant number 348327. We thank CSC – IT Center for Science for computational resources.

VII. REFERENCES

[1] X. Chen, X. Xie, P. Ruan, S. Liang, W.-Y. Wong, and G. Fang, ACS Energy Letters **0**, 2037 (2024).
[2] R. Feng, Y. Chen, X. Zhang, B. J. Rousseau, P. Gao, P. Chen, S. T. Mergelsberg, L. Zhong, A. Hollas, Y. Liang, V. Murugesan, Q. Huang, E. Walter, S. Hammes-Schiffer, Y. Shao, and W. Wang, Joule **7**, 1609 (2023).
[3] T. V. Sawant, C. S. Yim, T. J. Henry, D. M. Miller, and J. R. McKone, Joule **5**, 360 (2021).
[4] S. Srinivasan, *Fuel cells: from fundamentals to applications* (Springer Science & Business media, 2006).
[5] W. Mook, M. Aroua, and G. Issabayeva, Renewable and sustainable energy reviews **38**, 36 (2014).
[6] S. Grigoriev, V. Fateev, D. Bessarabov, and P. Millet, International Journal of Hydrogen Energy **45**, 26036 (2020).
[7] M. Seralathan and S. Rangarajan, Journal of Electroanalytical Chemistry and Interfacial Electrochemistry **191**, 209 (1985).
[8] C. Wiberg, M. Busch, L. Evenäs, and E. Ahlberg, Electrochimica Acta **367**, 137480 (2021).
[9] Q. Xu and T. Zhao, Progress in Energy and Combustion Science **49**, 40 (2015).
[10] G. L. Soloveichik, Chemical Reviews **115**, 11533 (2015), pMID: 26389560.
[11] A. Orita, M. Verde, M. Sakai, and Y. Meng, Journal of Power Sources **321**, 126 (2016).
[12] M. M. Cooper, H. Kouyoumdjian, and S. M. Underwood, Journal of Chemical Education **93**, 1703 (2016).
[13] T. Ree, Journal of Chemical Education **48**, 467 (1971).
[14] M. POURBAIX, Corrosion **6**, 395 (1950).
[15] E. L. Lebeau, R. A. Binstead, and T. J. Meyer, Journal of the American Chemical Society **123**, 10535 (2001), pMID: 11673985.
[16] S. Hammes-Schiffer, Chemical Reviews **110**, 6937 (2010), pMID: 21141827.
[17] G. A. Mabbott, Journal of Chemical Education **60**, 697 (1983).
[18] N. Elgrishi, K. J. Rountree, B. D. McCarthy, E. S. Rountree, T. T. Eisenhart, and J. L. Dempsey, Journal of Chemical Education **95**, 197 (2018).
[19] P. Chooto, Voltammetry. IntechOpen , 1 (2019).
[20] N. Navashree and P. Parthasarathy, MaterialsToday: Proceedings (2023), 10.1016/j.matpr.2023.05.175.
[21] G. Korotcenkov, S. D. Han, and J. R. Stetter, Chemical Reviews **109**, 1402 (2009), pMID: 19222198.
[22] J. J. Van Benschoten, J. Y. Lewis, W. R. Heineman, D. A. Roston, and P. T. Kissinger, Journal of Chemical Education **60**, 772 (1983).
[23] A. Hashemi, P. Peljo, and K. Laasonen, The Journal of Physical Chemistry C **127**, 3398 (2023).
[24] J. Kim and H. Park, Renewable Energy **138**, 284 (2019).
[25] V. Muralidharan, S. Jayasubramaniyan, and H.-W. Lee, EES. Catal. **2**, 522 (2024).
[26] E. Laviron and L. Roullier, Journal of Electroanalytical Chemistry and Interfacial Electrochemistry **186**, 1 (1985).
[27] M. Okubo, K. Kawai, Z. Ma, and A. Yamada, Accounts of Materials Research **3**, 33 (2022).
[28] A. Hashemi, R. Khakpour, A. Mahdian, M. Busch, P. Peljo, and K. Laasonen, Digital Discovery **2**, 1565 (2023).
[29] K. Burke, The Journal of Chemical Physics **136**, 150901 (2012).
[30] F. Giustino, *Materials modelling using density functional theory: properties and predictions* (Oxford University Press, 2014).
[31] K. Mathew, R. Sundararaman, K. Letchworth-Weaver, T. A. Arias, and R. G. Hennig, The Journal of Chemical Physics **140**, 084106 (2014).
[32] J. Rossmeisl, Z.-W. Qu, H. Zhu, G.-J. Kroes, and J. Nørskov, Journal of Electroanalytical Chemistry **607**, 83 (2007), theoretical and Computational Electrochemistry.
[33] M. Bursch, J.-M. Mewes, A. Hansen, and S. Grimme, Angewandte Chemie International Edition **61**, e202205735

(2022).
[34] R. P. Fornari and P. de Silva, Molecules **26** (2021), 10.3390/molecules26133978.
[35] M. Busch, E. Ahlberg, E. Ahlberg, and K. Laasonen, ACS Omega **7**, 17369 (2022).
[36] A. V. Marenich, C. J. Cramer, and D. G. Truhlar, The journal of physical chemistry. B **113 18**, 6378 (2009).
[37] A. Klamt, F. Eckert, M. Diedenhofen, and M. E. Beck, The journal of physical chemistry. A **107 44**, 9380 (2003).
[38] T. N. Brown and N. Mora-Diez, The journal of physical chemistry. B **110 18**, 9270 (2006).
[39] A. Hamza, F. B. Németh, Madarász, A. Nechaev, P. M. Pihko, P. Peljo, and I. Pápai, Chemistry – A European Journal **29**, e202300996 (2023).
[40] A. J. Bard, L. R. Faulkner, and H. S. White, *Electrochemical methods: fundamentals and applications* (John Wiley & Sons, 2022).
[41] in *Lead-Acid Batteries: Science and Technology*, edited by D. Pavlov (Elsevier, Amsterdam, 2011).
[42] M. J. Frisch, G. W. Trucks, H. B. Schlegel, G. E. Scuseria, M. A. Robb, J. R. Cheeseman, G. Scalmani, V. Barone, G. A. Petersson, H. Nakatsuji, X. Li, M. Caricato, A. V. Marenich, J. Bloino, B. G. Janesko, R. Gomperts, B. Mennucci, H. P. Hratchian, J. V. Ortiz, A. F. Izmaylov, J. L. Sonnenberg, D. Williams-Young, F. Ding, F. Lipparini, F. Egidi, J. Goings, B. Peng, A. Petrone, T. Henderson, D. Ranasinghe, V. G. Zakrzewski, J. Gao, N. Rega, G. Zheng, W. Liang, M. Hada, M. Ehara, K. Toyota, R. Fukuda, J. Hasegawa, M. Ishida, T. Nakajima, Y. Honda, O. Kitao, H. Nakai, T. Vreven, K. Throssell, J. A. Montgomery, Jr., J. E. Peralta, F. Ogliaro, M. J. Bearpark, J. J. Heyd, E. N. Brothers, K. N. Kudin, V. N. Staroverov, T. A. Keith, R. Kobayashi, J. Normand, K. Raghavachari, A. P. Rendell, J. C. Burant, S. S. Iyengar, J. Tomasi, M. Cossi, J. M. Millam, M. Klene, C. Adamo, R. Cammi, J. W. Ochterski, R. L. Martin, K. Morokuma, O. Farkas, J. B. Foresman, and D. J. Fox, "Gaussian 16 Revision C.01," (2016), gaussian Inc. Wallingford CT.
[43] P. C. Hariharan and J. A. Pople, Theoretica chimica acta **28**, 213 (1973).
[44] J. J. P. Stewart, Journal of Molecular Modeling **19**, 1 (2013).
[45] A. V. Marenich, C. J. Cramer, and D. G. Truhlar, The Journal of Physical Chemistry B **113**, 6378 (2009), pMID: 19366259.
[46] F. Weigend, F. Furche, and R. Ahlrichs, The Journal of Chemical Physics **119**, 12753 (2003).
[47] J. Ho and M. L. Coote, Theoretical Chemistry Accounts **125**, 3 (2009).
[48] J. Rodriguez, C. Niemet, and L. D. Pozzo, ECS Transactions **89**, 49 (2019).
[49] W. Li, J. Li, X. Yuan, Z. Xiang, Z. Liang, and Z. Fu, J. Mater. Chem. A **11**, 19308 (2023).
[50] C. S. Sevov, K. H. Hendriks, and M. S. Sanford, The Journal of Physical Chemistry C **121**, 24376 (2017).
[51] R. Chen, ChemElectroChem **6**, 603 (2019).
[52] S. Gentil, D. Reynard, and H. H. Girault, Current Opinion in Electrochemistry **21**, 7 (2020), energy Storage Energy Transformation.
[53] C. Flox, C. Zhang, and Y. Li, Current Opinion in Chemical Engineering (2023).
[54] R. Thomson, *Naturally occurring quinones* (Elsevier, 2012).
[55] N. R. Patel, "Phthalazines," in *Chemistry of Heterocyclic Compounds* (John Wiley Sons, Ltd, 1973) Chap. II, pp. 323–760.
[56] J. B. Laursen and J. Nielsen, Chemical Reviews **104**, 1663 (2004), pMID: 15008629.
[57] T. J. Haley, Clinical Toxicology **8**, 13 (1975), pMID: 805682.
[58] T. Vogler and A. Studer, Synthesis **2008**, 1979 (2008).
[59] C. Bird and A. Kuhn, Chemical Society Reviews **10**, 49 (1981).